Multiple-localized-exciton species in sulfide-doped AgBr detected by photoluminescence and optically detected magnetic resonance

M. S. Burberry, A. P. Marchetti, J. P. Spoonhower, W. G. McDugle, and R. H. D. Nuttall
Research Laboratories, Eastman Kodak Company, Rochester, New York 14650

D. S. Tinti
Department of Chemistry, University of California, Davis, California 95616
(Received 8 April 1991)

The low-temperature photoluminescence of sulfide-doped AgBr has been examined with both steady-state and pulsed excitation. Prominent emission bands are observed at about 495, 566, 596, and 725 nm, depending upon excitation conditions. Sub-band-gap excitation peaks are observed at 464, 482, 496, 530, and 558 nm, depending upon monitoring wavelength. Excitation at 496 nm preferentially enhances the 596-nm emission that gives rise to an optically-detected-magnetic-resonance (ODMR) spectrum. ODMR data indicate that at least three species are contributing to the 596-nm emission. These species are interpreted as triplet excitons. A highly anisotropic species observed in the ODMR spectra is interpreted as a triplet exciton bound to a substitutional divalent sulfur-ion–interstitial-silver-ion complex with approximate [111] symmetry.

I. INTRODUCTION

Nominally pure AgBr shows two "intrinsic" emission bands. It is generally accepted that the band at 495 nm is due to trace iodide impurity resulting in recombination of an iodide-bound exciton.[1–4] Assignments of the broader band at 580 nm have varied widely among investigators. It has been attributed to silver centers[5] and iodide-perturbed sulfide impurity ions.[6] More recently, it has been shown that the band is a superposition of donor-acceptor recombination and intermediate case exciton recombination.[7,8] The donor is believed to be either an interstitial silver ion or a substitutional divalent cation, and the acceptor is assigned to a silver-ion vacancy.

Doping silver halides with sulfide ions and other chalcogenides generates new centers. These have received considerable experimental attention, having been examined mainly with low-temperature optical and electron-paramagnetic-resonance (EPR) spectroscopies. As summarized in a recent review,[9] chalcogenide doping of AgCl and AgBr extends the optical absorption and photophysical activity to lower energies than the band-gap energy, modifies the intrinsic luminescence spectra of the nominally pure materials, and leads to EPR active species upon photoirradiation. However, the properties and other details of the centers generated remain largely unclear, most particularly for sulfide doping.

Hediger and Junod[10] have reported luminescence spectra at 4.2 K of sulfide-doped AgBr (AgBr:S) that show that sulfide doping quenches the "intrinsic" band of AgBr at 495 nm and causes the appearance of additional emission bands. The latter have maxima at 564 and 642 nm for samples with a nominal sulfide concentration of 60 mppm (molar parts per million). A shoulder at 596 nm appears at higher sulfide concentrations (120 mppm). Assignments of these bands were not made. Absorption and visible-infrared emission spectra at 77 K of Ag_2S sols, primitive silver halide emulsions, and $Na_2S_2O_3$-digested emulsions have been published.[6] It was found that sols and small particles of Ag_2S on microcrystal substrates emit in the range of 750–1200 nm. Peak wavelengths were found to be directly related to Ag_2S particle size, with larger particles emitting at longer wavelengths. Assignments for the 4.2-K emission bands of Hediger and Junod[10] were also suggested.[6] The 565-nm peak was assigned to "iodide–sulfide-ion pairs," the shoulder at 596 nm to "nearly isolated sulfide centers" compensated with an interstitial silver ion (although it was not explained why this species should appear only at the higher concentration), and the band at 640 nm to "weakly interacting sulfide pairs." However, the assignments were largely conjectures with little substantiating data.

A variety of EPR active centers have also been detected in sulfide-doped (and doubly doped) silver halides,[9] but the nature of these centers, and their relation to the luminescence, is not well understood. A better understanding exists for centers arising from selenide and telluride doping of AgCl and AgBr. Doping AgBr with Te^{2-} extended absorption beyond 650 nm.[11] EPR studies of polycrystalline AgBr and AgCl (Ref. 12) and single-crystal AgBr (Ref. 13) were interpreted in terms of monovalent Se^- and Te^- substituted at bromide lattice sites. More detailed investigations[14,15] in AgBr concluded that these centers were actually dimers. Two distinct defect centers were identified, depending upon the exposure temperature.[16] These species are isoelectronic with the V_k centers observed in alkali halides; they consist of Se_2^{3-} (or Te_2^{3-}) molecules with [110] orientation. Both centers are produced by photoionization of Se_2^{4-} (or Te_2^{4-}) dimers aligned along a [110] lattice direction and compensated by an adjacent interstitial Ag^+ ion. One center is also compensated by a bromide vacancy along the pseu-

domolecular axis. Analogous centers were identified in AgCl.[16]

Mononuclear chalcogen ions have been detected by exposing crystals which have also been doped with divalent cations.[17–19] Cadmium and copper in combination with sulfide, selenide, and telluride have been investigated. Studies of AgCl doubly doped with silver sulfide and mercury(I) or mercury(II) chloride have also been reported.[20] EPR spectra of oxygen-doped AgBr crystals indicated that a center possessed axial symmetry along a [100] direction.[21]

Here we report the results of further investigation into the photophysics of sulfide-ion-doped AgBr, focusing on lower dopant concentrations than earlier studies. Emission, photoexcitation, and optically-detected-magnetic-resonance (ODMR) spectra are reported.

II. EXPERIMENT

A. Sample preparation

Crystals of AgBr and sulfide-doped AgBr were prepared using conventional Bridgman techniques as described previously.[7] Ag_2S (2–200 mppm) was added as a dopant to the precipitate before melting. Samples from the boule were cut and polished. Samples were examined either unannealed (as grown) or annealed at 350 °C in air for times ranging from 15 h to several days. Annealed samples were cooled to ambient temperature and then placed in the cryostat for measurement. Samples containing higher concentrations of sulfide (200 mppm) were visually inhomogeneous. At lower concentrations some evidence for domain formation or twinning was revealed in the ODMR spectra. Specimens were analyzed for impurities using the methods of inductively coupled plasma-mass spectroscopy, graphite furnace atomic absorption, and ion-coupled plasma optical-emission spectroscopy. A number of elemental impurities including Cl, I, Fe, Ni, Cr, Cu, Cd, Cs, Mg, and Sn were all found to be present at levels below 1 mppm. The incorporation of sulfur was confirmed in the sample with a formal concentration of 5 mppm by accelerator mass spectrometry. The actual concentration of incorporated sulfide ion remains unknown and is reported as the formal concentration used in growing the crystals.

B. Optical spectroscopy

The temperature dependence of the visible luminescence was investigated between 2 and 100 K. Only small variations in band intensities are observed below 6 K. At temperatures approaching 77 K, however, the emission bands become considerably weaker, shifts to longer wavelength occur, and the bands broaden. Exposure at 100 K causes irreversible loss of the luminescence. The reported emission and photoexcitation spectra were obtained at ≤ 6 K on samples that had not been exposed previously. The emission spectra were recorded with a 1-m Jarrel Ash Czerny-Turner spectrometer equipped with a cooled RCA C31034 GaAs photomultiplier tube. Steady-state excitation spectra were obtained with a 450-W xenon arc lamp in conjunction with a modified Cary 14 scanning monochromator. The emission and excitation spectra are corrected for the wavelength dependence in the emission spectrometer response and in the excitation source respectively, unless noted otherwise. Selected cw excitation wavelengths were provided by argon-ion and helium-cadmium lasers. Photomultiplier signals were analyzed using phase-sensitive detection with the chopper positioned after the sample. Cutoff (interference) filters were placed between the sample and detector, where appropriate, to eliminate second-order transmission and stray light from the emission (excitation) spectra.

The evolution of the luminescence after pulsed excitation was examined by two methods. The first employed a gated photon counter with selectable gate width and delay time to process the photomultiplier signal from the scanning emission monochromator. A second method used a programmable digitizer to acquire decay curves at particular monitoring wavelengths. Pulsed excitation was provided by a nitrogen laser (337 nm) or nitrogen-laser-pumped dye laser in both sets of experiments.

C. ODMR spectroscopy

Samples for ODMR measurements were aligned by x-ray back reflection and mounted in the center of a split-coil superconducting magnet. The crystals were excited with either the 458- or 488-nm line of an air-cooled Ar^+ laser. Emission was observed at right angles to the excitation with a lens-filter combination and a red-sensitive photomultiplier; the output of the photomultiplier was fed to a lock-in amplifier. Either a combination of Corning glass filters or a compact monochromator was employed to determine the emission wavelength dependence of the ODMR transitions. Microwave radiation (36 GHz) was applied to the sample from a two-cavity klystron (5 W maximum) through a circular stainless-steel waveguide, the end of which was positioned less than $\lambda/2$ from the sample. A *p-i-n* diode was used to amplitude modulate the microwaves. Magnetic-field sweep and data acquisition were controlled by a computer. Calibration was achieved by observing resonances from diphenyl picryl hydrazyl.

Additional ODMR spectra were obtained using a custom Oxford Instruments SM4 cryomagnet system in which crystals were placed at the center of a split-coil superconducting magnet in a 24-GHz microwave cavity with large optical access. A *p-i-n* diode modulator was used to amplitude-modulate the microwaves. A maximum power of 600 mW was available from the klystron oscillator. ODMR signals, monitored along the magnetic-field direction, were detected as changes in the luminescence intensity by a Hammamatsu R375 photomultiplier tube. In these experiments emission was excited using the unfocused output of an Ar^+ laser; power levels of 50 mW were typical.

Zero-field ODMR spectra in the range 0.1–18 GHz were obtained on an apparatus which has been previously described.[22] Zero-field spectra were recorded on both annealed and unannealed crystals of AgBr doped with 5 mppm sulfide and detected using a red-sensitive pho-

tomultiplier tube with long pass filters that transmitted wavelengths beyond 580 nm.

III. RESULTS

A. Steady-state luminescence spectra

The low-temperature emission spectra were examined at several excitation wavelengths above and below the 2.681-eV (462-nm) indirect exciton band edge of AgBr. Figure 1 shows typical corrected low-temperature photoluminescence spectra (2 K) at a variety of excitation wavelengths for an unannealed silver bromide single crystal doped with 5 mppm sulfide. Curves are normalized at their peaks and offset vertically to facilitate comparison. Similar spectra were obtained for crystals containing 20 mppm sulfide.

The spectra depend markedly on the wavelength of excitation. Excitation at 325 nm results in a weak emission band at 495 nm associated with the iodide-bound exciton and intense bands at 570 and 725 nm. Lengthening the excitation wavelength to 458 nm results progressively in loss of the 495- and 725-nm bands and a narrowing and concomitant blue shift of the 570-nm band to 566 nm. Further spectral features appear with excitation at even longer wavelengths, most notably a band at 596 nm that appears with 488-nm excitation. The 596-nm band is lost and a weak band at 650 nm appears with 515-nm excitation. The large changes seen in the emission spectra with excitation imply that a large variety of emissive centers are present in AgBr:S, even at 5 mppm.

The emission spectra are considerably simplified in annealed samples of AgBr:S. As shown in Fig. 2 for 5 mppm doping, air annealing (350 °C, 15 h) favors the emission band at 596 nm and quenches the bands at 566 and 725 nm for excitation both above and below the indirect edge of AgBr. Hence air annealing appears to reduce the number of emissive centers present in melt-grown AgBr:S crystals. Table I summarizes the emission maxima observed for different excitations in both unannealed and air-annealed samples. Some data are included for a crystal doped at 20 mppm.

Treatments other than air annealing have variable effect. Etching either air-annealed or unannealed samples with cyanide in an attempt to remove possible surface species has no consequence on the emission spectra. However, annealing samples in a bromine atmosphere (350 °C, 15 h) causes the emission spectra to become indistinguishable from those of undoped AgBr.

B. Transient luminescence spectra

Emission spectra of AgBr:S crystals were recorded following pulsed excitation at 488 nm as a function of delay time. Spectra for an unannealed sample are shown in Fig. 3 for gate delays of 0, 0.2, and 1.0 ms with observation windows of 5 μs, 0.2 ms, and 1.0 ms, respectively. Arbitrary normalization factors have been applied to the spectra in Fig. 3 to facilitate comparison. Bands are observed at 562 and 596 nm with zero delay. The relatively

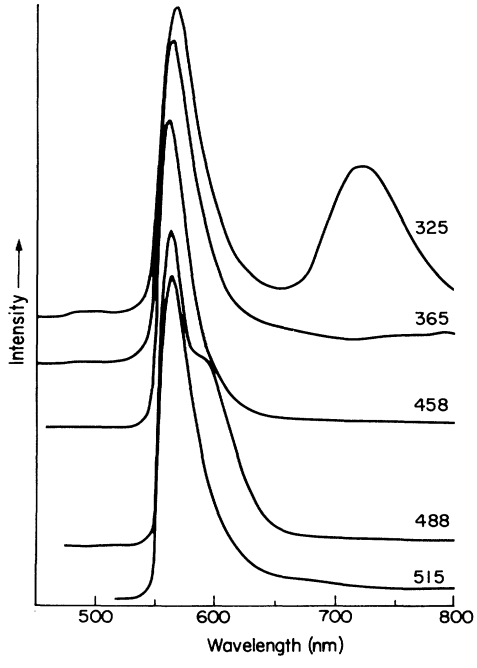

FIG. 1. Steady-state photoluminescence spectra of an unannealed crystal excited at the laser wavelengths indicated in nm. 365-nm excitation was from a lamp and monochrometer combination. All luminescence spectra in this and the following figures were obtained at 2.0 K from AgBr single crystals doped with 5 mppm sulfide.

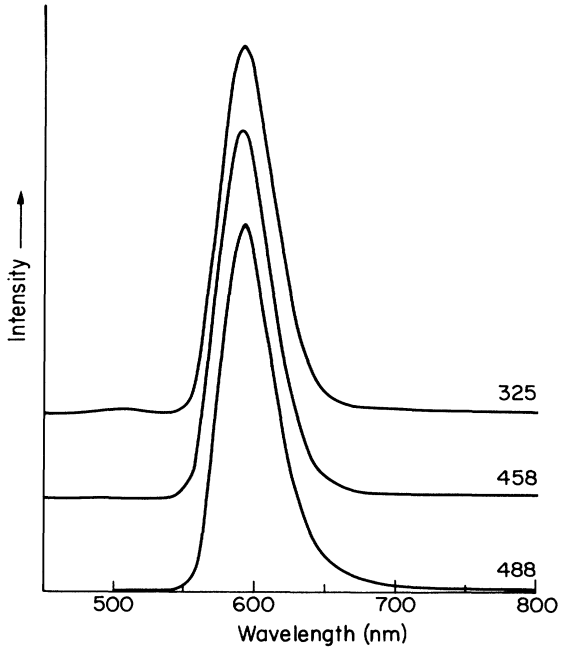

FIG. 2. Steady-state photoluminescence spectra of a doped crystal after annealing in air at 350 °C for 15 h. The laser excitation lines used are indicated in the figure in nm.

TABLE I. Emission bands for sulfide-doped AgBr at discrete excitation wavelength.

Sample	Excitation λ (nm)	Emission peak λ (nm)				
Unannealed	325	495[a]	570[b]		725	
(5 mppm)	365	495[c]	568[b]		650[a]	775[a]
	458		566			
	488		566	596		
	515		566		650[a]	
Unannealed	325	500	567[b]			725
(20 mppm)	365		566[b]		650	775
	458		564		650[a]	
	488		564	596	650[a]	
	515		564		650[a]	
Annealed	325	495[c]	596			
(5 mppm)	458		596			
	488		596			

[a] Weak.
[b] Broad long-wavelength tail.
[c] Very weak.

sharp band at 562 nm exhibits nonexponential decay and shifts to longer wavelength by $+5\pm1$ nm for a delay of 0.3 ms. This band is relatively short lived and, essentially, is not seen for delays >1 ms. The shift of the maximum with time and the nonexponential decay of the 562-nm band are suggestive of a donor-acceptor recombination. The longer-lived emission at 596 nm also exhibits a nonexponential decay, but it does not appear to shift with time. The shift of the long-wavelength maximum in the 0.2-ms spectrum is due to a third band at 587 nm, which is resolved at intermediate times. The 596-nm band is evident as an inflection on the long-wavelength tail of this third band.

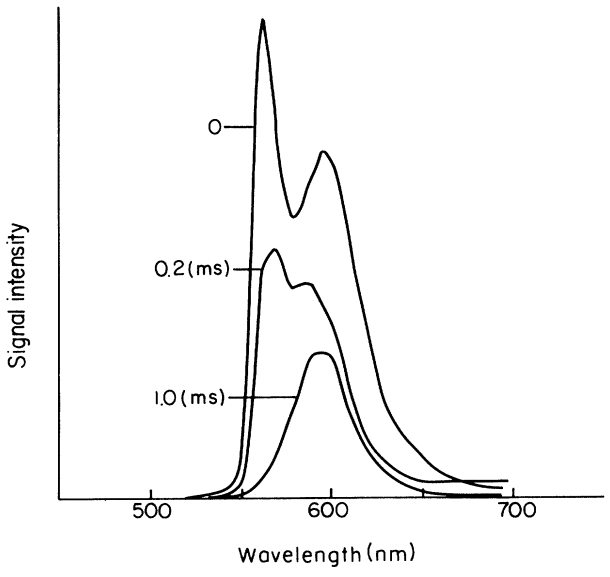

FIG. 3. Time-resolved spectra of an unannealed crystal excited at 488 nm, obtained usinng a gated photon counter. Gate delays were 0, 0.2, and 1.0 ms, as indicated in the figure. The corresponding gate widths were 50 μs, 0.2 ms, and 1.0 ms, respectively.

C. Steady-state excitation spectra

Representative excitation spectra monitoring the major features in the emission are shown in Fig. 4. Contrary to results for undoped AgBr, for which no excitation bands are detected at lower energies than the indirect gap, several bands appear in this region for sulfide-doped samples. The most prominent bands occur at 466, 496, and 530 nm for both unannealed and air-annealed samples. However, the 496-nm band is greatly enhanced in air-annealed samples when detecting at 600 nm, suggesting

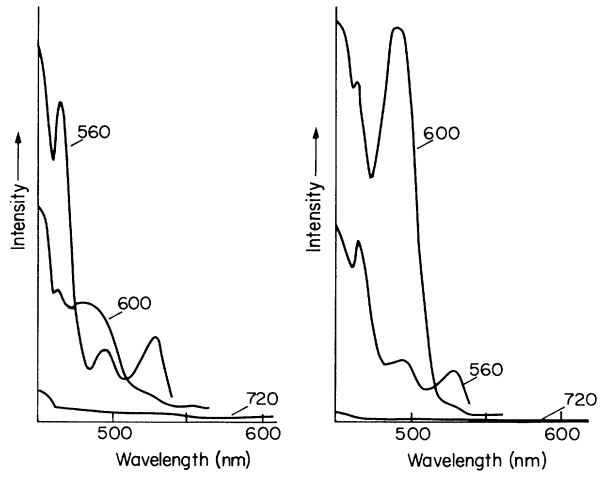

FIG. 4. Steady-state photoexcitation spectra of (a) unannealed and (b) annealed sulfur-doped AgBr crystals monitored at 560, 600, and 720 nm, respectively.

TABLE II. Sub-band-gap excitation bands for sulfide-doped AgBr at discrete monitoring wavelength.

Sample	Excitation peak λ (nm)					Monitoring λ (nm)
Unannealed	464	496	530			560
(5 mppm)	464[a]	482	530[a]			600
	b					720
Unannealed	464	496	525			580
(20 mppm)	471	489	514[a]	542		600
	b	496[c]		540		690
	b	502		537	558	800
Annealed	464	496	530			560
(5 mppm)	464[a]	496	530[a]			600
	b					

[a] Weak.
[b] Broad tail extending below the band gap.
[c] Very weak.

that the 496-nm band in excitation and 596-nm band in emission relate to the same species. No distinct, sub-band-gap excitation bands are seen monitoring at 720 nm. The observed sub-band-gap excitation bands are summarized in Table II. Data obtained on a crystal doped at 20 mppm are also included.

D. ODMR

High-field ODMR spectra at 36 GHz of an unannealed 5-mppm sulfide-doped AgBr crystal at 1.9 K are shown in Fig. 5 for two modulation frequencies with the magnetic field parallel to the [111] crystal direction. Comparison of the [111] spectra in Fig. 5 shows different dependences on modulation frequencies for different features in the spectra. The outer, highly anisotropic features at 1.0–1.4 and 1.6–2.0 T are more intense at high modulation frequencies (2 kHz), while the central, less anisotropic features at 1.4–1.6 T are more intense at low modulation frequencies (200 Hz). Both outer and central regions have the same emission and excitation wavelength dependences; namely, the signals in both regions are associated with the emission band at 596 nm and the excitation band at 496 nm. Air-annealed samples yield a relatively stronger central region, by a factor of about 5 at a given modulation frequency, and possibly some weak new lines in this region. However, in general, the ODMR spectra of unannealed and air-annealed samples for dopant concentrations ≤ 5 mppm are similar. The resonance fields for rotation in a (110) plane are summarized in Fig. 6. These show clearly that extrema occur for the magnetic field oriented near [111].

ODMR spectra were recorded at 24 and 36 GHz. For a given field orientation, the peak spacings were almost identical, indicating that the splittings are due to fine structure or (less likely) to hyperfine structure. Examination of light emission during microwave modulation indicates that the light intensity increases when the microwaves are turned on, so that the major ODMR resonances are positive. Although single crystals of sulfide-doped AgBr sometimes gave evidence of twinning or

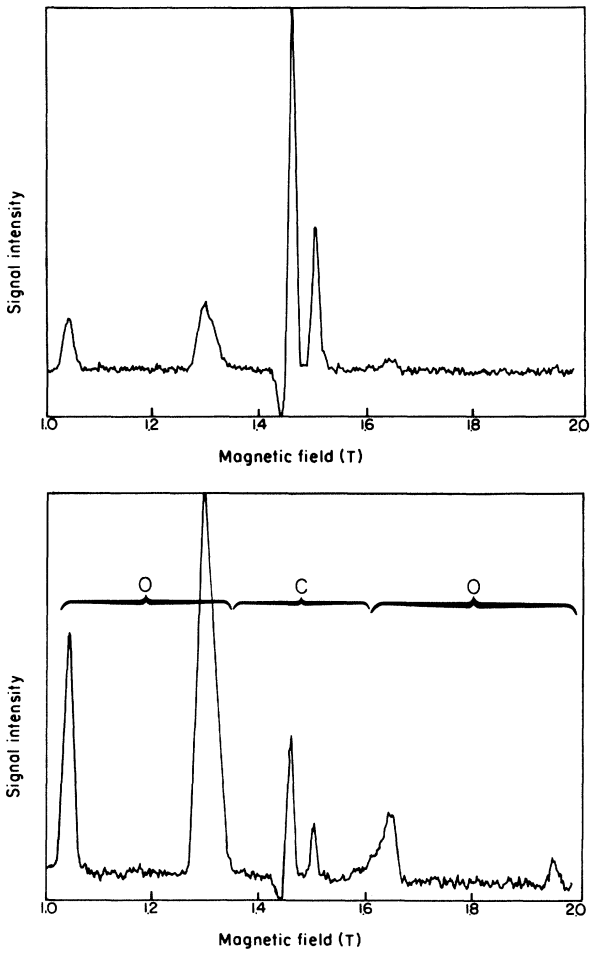

FIG. 5. ODMR spectra of an unannealed crystal of AgBr doped with 5 mppm sulfide at 1.9 K with the magnetic field parallel to [111]. The microwave modulation frequencies were 200 (upper) and 2000 Hz (lower). The excitation wavelength was 488 nm, the luminescence was monitored at 600 nm through a broadband filter, and the microwave frequency was 35.98 GHz.

domain formation, good ODMR spectra for [111] and [110] orientations of the magnetic field with respect to the crystal axes have been obtained. Data for a [100] orientation of the magnetic field were always poorer, with decreased signal-to-noise ratio.

The zero-field ODMR spectra of a 5-mppm AgBr:S crystal exhibited a large number of positive resonances at 1.4 K with complex and somewhat variable structure. In the low-frequency range (0.1–4.0 GHz), signals occur at 0.59, 1.4, and 1.9 GHz. The 1.9-GHz signal is the most intense at low modulation frequencies (100 Hz), while the 0.59-GHz signal is the most intense at high modulation frequencies (1 kHz). The available signal-to-noise ratio allowed the recording of an action spectrum only for the 1.9-GHz resonance. This peaked at 595±5 nm. At higher frequency the stronger signals occurred at 5.7, 12.3, 14.4, and 15.1 GHz, but many other weaker signals were detected between 4 and 18 GHz. The spectra did not significantly differ between unannealed and air-annealed samples. Although spectra were not obtained for higher dopant concentrations, the signals noted are not seen in undoped samples.

IV. DISCUSSION

The emission spectra of sulfide-doped silver bromide are much richer than those that have previously been reported. Overall, the results indicate that even at dopant levels as low as 5 mppm a number of sulfide-related species are present. Emission from these centers competes effectively with the intrinsic emission of AgBr. In particular, emission at 495 nm due to the iodide-bound exciton is quenched in 5 mppm AgBr:S for excitation wavelengths longer than 365 nm. A number of sub-band-gap excitation peaks are associated with sulfide-related emission bands. Absorption at 466 and 530 nm leads to 566-nm emission, while the 596-nm emission is preferentially excited by absorption at 496 nm. The high-field ODMR spectra are associated primarily with the 596-nm emission band. However, the complexity of the ODMR spectra requires contributions from more than a single ODMR active species, so that the 596-nm band does not proceed from a single emissive center.

A possible model for the ODMR active centers in AgBr:S involves sulfide-bound excitons, formed either directly from optical excitation or by sequential capture of, say, a hole and then an electron. A variety of exciton species are known in AgBr and AgCl, including the iodide-bound exciton in AgBr (Refs. 3 and 23) and AgCl,[24] the self-trapped exciton and self-trapped exciton with a bromide in the first shell in AgCl,[22,25,26] and the intermediate case exciton in AgBr.[8] All of these excitons, which have binding energies >40 meV, are neutral with respect to the lattice. It should also be noted that free excitons can be weakly bound (<8 meV) at neutral or ionized donors.[27] Two types of simple sulfide species that would be charge neutral are substitutional monomeric sulfide S^{2-}, compensated by an interstitial silver ion, a substitutional divalent cation impurity, or a bromide ion vacancy, and substitutional sulfide pairs S_2^{4-}, fully compensated with bromide vacancies and/or interstitial silver ions. The sulfide pairs are analogous to the parent X_2^{4-} (X=Se and Te) centers that yield EPR active X_2^{3-} centers in photoirradiated selenide- and telluride-doped AgBr.[14–16] A single substitutional sulfide would have [111] symmetry when compensated with a nearest-neighbor interstitial silver ion, [100] symmetry when compensated with a next-nearest-neighbor bromide vacancy, and [110] symmetry when compensated with a nearest-neighbor bromide vacancy. The fully compensated sulfide pair ($S_2^{4-}V_{Br}Ag_i$) would have approximate [110] symmetry.

The rotation data in Fig. 6 indicate near [111] symmetry for the outer resonances. These are accordingly tentatively assigned to the triplet state of an exciton consisting of a single sulfide compensated by an interstitial silver ion. The triplet-state assignment is consistent with the similar splittings seen at 24 and 36 GHz and with the observation of half-field transitions between 0.65 and 0.75 T at 36 GHz and a weak level anticrossing (LAC) resonance at 0.45 T.

The spin Hamiltonian for a triplet-state species in a Zeeman field is

$$\mathcal{H}=\mu_B \mathbf{S}\cdot\overleftrightarrow{g}\cdot\mathbf{B}+\mathbf{S}\cdot\overleftrightarrow{D}\cdot\mathbf{S}\ , \tag{1}$$

where the first term represents the Zeeman interaction

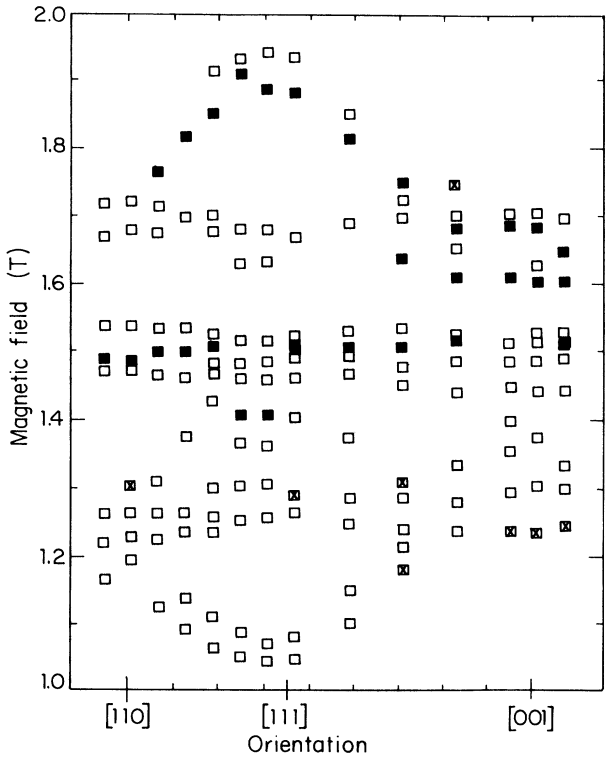

FIG. 6. Variation of the ODMR resonances as a function of the magnetic-field direction in the (110) crystal plane. The open squares are positive resonances, the solid squares are negative resonances, and the crossed squares represent very weak resonances. These data were obtained on an unannealed sample.

TABLE III. g factors and fine-structure constants obtained from the ODMR data.

Center assignment	$g_{\parallel}$	$g_{\perp}$	D (GHz)	E (GHz)
$S^{2-}Ag_i$	1.725	1.725	10.82±0.2	1.7±0.4
M-S	1.751	1.765	0.69±0.09	0
$S_2^{4-}V_{Br}Ag_i$?	≈1.74		<2.0	?

and the last term the fine-structure interactions $[D(S_Z^2-\frac{2}{3})+E(S_X^2-S_Y^2)]$. By convention, D and E will be expressed in frequency units (energy/h, where h is Planck's constant). Comparison of the rotation data with calculations of the resonance fields for various choices of parameters shows that rigorous [111] symmetry does not apply to the outer resonances. Rather, the data for the outer resonances indicate that the principal z axis is close to [111] with $|D|\approx 11$ GHz and $g\approx 1.72$, but that E is nonzero.

The available rotation data for these highly anisotropic lines, shown in Fig. 6, have been compared to angular dependences simulated for $\overleftrightarrow{D}$ with various principal-axis orientations using a computer program that employs numerical diagonalization of $\mathcal{H}$. The simulation accounted for the symmetry-related sites appropriate for the cubic lattice.[28,29] The data are most consistent with the presence of the "unique" principal direction of $\overleftrightarrow{D}$ close to [111]. Simulations with the orientations of the other principal directions varied in the plane perpendicular to [111] were also considered. Some fitting of the most reliable spectra, obtained with **B** along the [100], [110], and [111] directions, was used as a guide. This process was made difficult by the broad, overlapping transitions observed at many magnetic-field orientations. A calculated rotational plot that roughly accounts for the outer lines in the vicinity of [111] is shown in Fig. 7. The g factors and fine-structure constants for this and other centers are given in Table III.

The rotation data for the less anisotropic and less-resolved central region of the high-field ODMR spectra are shown in Fig. 8. The results appear to be due to two additional triplet-state species with g factors between 1.72 and 1.76. One species has axial symmetry [100] with $D\approx 0.69$ GHz. Figure 8 includes the fitted rotation curves for this species. The other species appears to have symmetry close to [110], based on the rotational plot extrema, with $D<2$ GHz and $g\approx 1.74$. Based on the symmetries of the simple sulfide centers considered earlier, the species with axial symmetry is tentatively assigned to a substitutional sulfide compensated by a divalent cation or less likely, a next-nearest-neighbor bromide vacancy. The species with near [110] symmetry is similarly assigned to a compensated sulfide dimer.

The species proposed as responsible for the major part

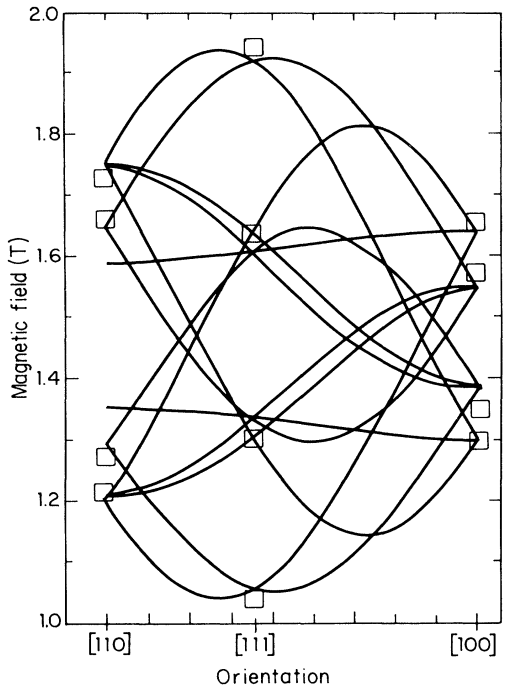

FIG. 7. The "best" simulation of the outer resonances shown in Fig. 6. The squares are data taken from the best spectra, with the magnetic field along [110], [111], and [100] directions. The parameters for this simulation are given in Table III.

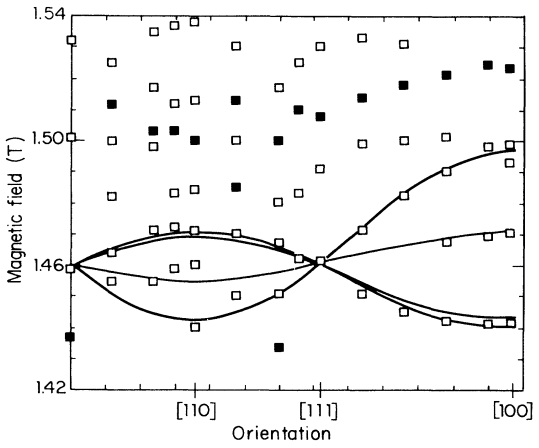

FIG. 8. Variation of the ODMR resonances in the central region as a function of magnetic-field direction in the (110) crystal plane. The solid squares are negative resonances. These data were obtained on an annealed crystal. The solid lines are a fit to an axial species whose parameters are given in Table III.

of the high-field ODMR spectra are consistent with the types of sulfide species expected to bind triplet excitons, with the types of species that have been deduced from EPR data in irradiated chalcogenide-doped AgBr and AgCl (Refs. 14–19) and with the annealing data if migration of species at elevated temperatures leads to an increase in the number of metal-sulfur pairs and sulfur aggregates.

The range of g factors found are reasonable for sulfide-bound excitons. Several centers have been observed in the EPR spectra of optically exposed sulfide-doped AgBr.[12,13,30] These centers have g factors of 2.02 ± 0.01 and can be interpreted as holes trapped at sulfide dimers, in analogy to the observations in selenide- and telluride-doped AgBr.[14–19] Taking the g factor as indicative of a sulfide-based holes ($g_h=2.02\pm0.01$) and $g_e=1.493$ for electrons in AgBr,[31] an approximate g factor for the sulfide-based exciton is given by the arithmetic average of the electron and hole g factors,[32]

$$g_{\rm ex}=(g_e+g_h)/2 \ . \tag{2}$$

This yields $g_{\rm ex}\approx1.75$, in reasonable agreement with the 1.72–1.77 range given in Table III.

The zero-field ODMR results also indicate a variety of sulfide-related centers in 5 mppm AgBr:S. Three resonance frequencies are anticipated for a given triplet-state species at zero field, corresponding to $2|E|$, $|D+E|$, and $|D-E|$. Among the many signals observed at zero field, no evident assignment of three frequencies to a given triplet-state species is possible within the measurement uncertainties for the relatively broad and structured signals. The three resonances at 0.59, 1.4, and 1.9 GHz might represent a single triplet-state species with $|D|=1.65$ and $|E|\approx0.3$ GHz, but alternate groupings of three frequencies are possible with only slightly larger errors in the three frequencies. Alternate groupings include the signals at 1.9, 12.3, and 14.4 GHz ($D\approx14.8$, $E\approx0.95$ GHz) and the signals at 0.59, 14.4, and 15.1 GHz ($D\approx14.8$, $E\approx0.3$ GHz). The first postulated grouping would agree with high-field results that suggest $|D|<2$ GHz for the triplet state of the compensated S_2^{4-} dimer. The latter two groupings are not consistent with any of the centers assigned at high field. The zero-field resonance at 0.59 GHz is also within experimental error of the high-field values of $D=0.69$ and $E\approx0$ found for the center with [100] symmetry. However, the foregoing is largely speculative; the assignments of the zero-field ODMR signals and their relationship to the high-field results remains unclear.

Since the high-field ODMR resonances are interpreted as arising from triplet recombination associated with the 596-nm emission band, we would like to identify the corresponding singlet emission from these centers if it exists. Excitation above the band gap is believed to produce free carriers that coalesce to form free excitons or are trapped to form excited-state donors, acceptors, and/or bound excitons. Bound singlet and triplet excitons should be formed in a 1:3 ratio with above-band-gap excitation. Triplet transitions are spin forbidden; therefore, direct absorption of below-band-gap excitation by the localized centers will preferentially produce singlet excited states. These states should emit, corresponding to singlet recombination, unless the intersystem crossing rate is unusually high.

The 566-nm emission band is ruled out as the singlet analog of the 596-nm band since annealing quenches the band. Annealing can alter the population distribution of defects, but is not expected to affect greatly the ratio of singlet emission to triplet emission. The 596-nm emission is nonexponential and is only roughly biexponential, with components of $\approx5\times10^{-5}$ and $\approx2\times10^{-3}$ s at 2 K. The zero- and high-field ODMR signals respond to modulation times on the order of 10^{-2} and 10^{-3} s; it is proposed that the broad 596-nm emission band represents unresolved singlet and triplet recombination. The temperature dependence of the decay kinetics of the band supports this idea. As the temperature is increased from 2 K, the relative intensity of the longer-lived component decreases in intensity. This may imply a small singlet-triplet splitting with Boltzmann equilibrium increasing the relative population of the higher-lying singlet state at higher temperatures. However, the interpretation is clouded by the fact that a variety of centers apparently contribute to the 596-nm emission.

The time-resolved emission data shown in part in Fig. 3 afford a strong argument for the assignment of the 566-nm band to a donor-acceptor recombination. This band shifts to longer wavelengths with delay time, a characteristic of donor-acceptor recombination.[33] The shift is $+5\pm1$ nm for a 0.3-ms delay. This assignment calls into question the previous suggestion of an interaction between iodide and sulfide.[10] The excitation bands at 464 and 530 nm (see Fig. 4) associated with the 566-nm emission could represent valence-band–to–donor and acceptor–to–conduction-band transitions, respectively. This would imply a donor trap depth of about 25 meV (estimated from the long-wavelength edge of the excitation band) and an acceptor trap depth of 375 meV. The donor depth is within experimental error of trap depths measured for weakly bound electrons in AgBr.[34–36] The acceptor depth would be an adiabatic value that is similar to estimates for other hole traps in AgBr.[9] High-field ODMR signals due to the donor and acceptor are not detected, presumably because of the short average recombination time evident from Fig. 3 for the 566-nm band.

V. CONCLUSIONS

Sulfide-doped AgBr exhibits a complex set of low-temperature photophysical processes that are manifest by a variety of optical-emission and excitation bands. The two most prominent emission bands, at 566 and 596 nm, are assigned to donor-acceptor recombination and to singlet and triplet exciton, emission, respectively. The 566-nm emission arises strongly from excitation of the 462- and 530-nm absorptions. The 596-nm emission arises from excitation of the 496-nm absorption. ODMR spectra are obtained by monitoring the 596-nm emission.

One ODMR active species is a triplet exciton, which is thought to be bound to a substitutional sulfide ion compensated by an interstitial silver ion. Other ODMR active species are tentatively assigned to excitons bound to compensated substitutional sulfur dimer and to divalent cation-sulfur pairs.

ACKNOWLEDGMENTS

The authors wish to thank Dr. Raymond Eachus for many discussions, suggestions, and contributions to this work. We thank Professor J. A. Weil for providing the computer program used for the simulation of magnetic-resonance data.

[1]H. Kanzaki and S. Sakuragi, J. Phys. Soc. Jpn **27**, 109 (1969).
[2]F. Moser and S. Lyu, J. Lumin. **3**, 447 (1971), and references cited therein.
[3]W. Czaja and A. Baldereschi, J. Phys. C **12**, 405 (1979).
[4]A. P. Marchetti and D. S. Tinti, Phys. Lett. **69A**, 353 (1979).
[5]A. J. B. Codling, Photogr. Sci. Eng. **19**, 44 (1975).
[6]C. T. Mumaw, Soc. Photogr. Sci. Eng. **24**, 87 (1980), and references cited therein.
[7]M. Burberry and A. Marchetti, Phys. Rev. B **32**, 1192 (1985).
[8]A. P. Marchetti, M. Burberry, and J. P. Spoonhower, Phys. Rev. B **43**, 2378 (1991).
[9]J. P. Spoonhower and A. P. Marchetti, J. Phys. Chem. Solids **51**, 793 (1990).
[10]H. Hediger and P. Junod, Soc. Photogr. Sci. Eng. **20**, 50 (1976), and references cited therein.
[11]C. Volke, Ann. Phys. (N.Y.) **6**, 203 (1956).
[12]I. Ebert, Z. Naturforsch. A **15**, 279 (1960).
[13]J. Busse and K. Hennig, Phys. Status Solidi **7**, K83 (1964).
[14]M. Höhne and M. Stasiw, Phys. Status Solidi **20**, 657 (1967).
[15]M. Höhne and M. Stasiw, Phys. Status Solidi **20**, 667 (1967).
[16]M. Höhne and M. Stasiw, Phys. Status Solidi **24**, 591 (1967).
[17]D. Schwarz, Phys. Status. Solidi **36**, 143 (1969).
[18]D. Schwarz, Phys. Status Solidi **37**, 197 (1970).
[19]D. Schwarz, Phys. Status Solidi B **48**, K61 (1971).
[20]S. Sonoike, M. Matsui, and K. Morimoto, Jpn. J. Appl. Phys. **11**, 247 (1972).
[21]M. Höhne, K. H. Segsa and M. Stasiw, Phys. Status Solidi **35**, 717 (1969).
[22]A. P. Marchetti and D. S. Tinti, Phys. Rev. B **24**, 7361 (1981).
[23]Y. Burki and W. Czaja, Europhys. Lett. **10**, 55 (1989).
[24]F. Moser, R. K. Ahrenkiel, and S. L. Lyu, Phys. Rev. **161**, 897 (1967).
[25]W. Hayes, I. B. Owen, and P. J. Walker, J. Phys. C **10**, 1751 (1977).
[26]N. Sugimoto, H. Yoshioka, and M. Yamaga, J. Phys. Soc. Jpn. **54**, 4331 (1985).
[27]W. von Osten and H. Stoltz, J. Phys. Chem. Solids **51**, 765 (1990).
[28]J. R. Morton and K. F. Preston, J. Magn. Reson. **52**, 457 (1983).
[29]J. A. Weil, T. Buch, and J. E. Clapp, Adv. Magn. Reson. **6**, 183 (1973).
[30]R. S. Eachus, W. G. McDugle, and M. T. Olm (unpublished).
[31]A. P. Marchetti, J. Phys. C **14**, 961 (1981).
[32]For example, J. Owen and E. A. Harris, in *Electron Paramagnetic Resonance,* edited by S. Geschwind (Plenum, London, 1972), Chap. 6.
[33]J. I. Pankoe, *Optical Processes in Semiconductors* (Dover, New York, 1971).
[34]R. C. Brandt and F. C. Brown, Phys. Rev. **181**, 1241 (1969).
[35]R. C. Brandt, D. M. Larsen, P. P. Crooker, and G. B. Wright, Phys. Rev. Lett. **23**, 240 (1969).
[36]S. Sakuragi and H. Kanzaki, Phys. Rev. Lett. **38**, 1302 (1977).